Ultrasonics Sonochemistry 99 (2023) 106550

Contents lists available at ScienceDirect

Ultrasonics Sonochemistry

journal homepage: www.elsevier.com/locate/ultson

Fast g-C_3N_4 sonocoated activated carbon for enhanced solar photocatalytic oxidation of organic pollutants through Adsorb & Shuttle process

Meriem Mergbi [a], Dominic Aboagye [b], Sandra Contreras [b], Hedi Ben Amor [a], Francisco Medina [b], Ridha Djellabi [b,*]

[a] Faculty of Sciences of Gabes, RL Processes, Energetic, Environment and Electric Systems (PEESE), University of Gabes, 6072 Gabes, Tunisia
[b] Department of Chemical Engineering, Universitat Rovira i Virgili, 43007 Tarragona, Spain

ARTICLE INFO

Keywords:
Ultrasonic synthesis
g-C_3N_4 coated AC
Biomass valorization
Solar photocatalysis
Adsorb & shuttle process

ABSTRACT

To solve low mass transfer in photocatalytic technology for water treatment, the combination of photoactive nanoparticles with highly adsorptive materials has been regarded as a successful approach. The optimization of photoactive particle coating in terms of dispersion on the surface of adsorbing support is the main key to reach a maximum synergism for pollutants removal. This study discusses the coating of as-prepared biomass based activated carbon by g-C_3N_4 using three routes, namely ball milling (AC-CN@BM), physical stirring (AC-CN@Phy) and ultrasonic assisted coating (AC-CN@US). The coating mechanisms by different processes were discussed using different characterization techniques. Ball milling based coating provides good g-C_3N_4 dispersion on the surface of AC, however, a partial degradation of g-C_3N_4 structure and a lower surface area were confirmed by FTIR, XRD and BET analysis. Physically designed sample shows a significant agglomeration of particles on the surface of AC. However, ultrasonic coating provides excellent distribution of g-C_3N_4 and high surface of the composite. In terms of photoactivity, AC-CN@BM exhibits the lowest adsorption and photocatalytic activity under solar light for the removal of ciprofloxacin. AC-CN@Phy showed medium performance, but less physical stability of g-C_3N_4 particles on AC, leading to their partial release. AC-CN@US showed the highest efficiency and stability after using; suggesting the good combination between g-C_3N_4 and AC, which in turn maximizes the removal of ciprofloxacin via Adsorb & shuttle process. The overall costs of composite, including the starting elements and the coating ultrasonic process are relatively low and green as compared to commonly reported routes.

1. Introduction

Photocatalysis has been widely investigated as an emerging route towards environmental and energy related applications [1,2]. It focuses on the activation of photocatalyst with light energy which leads to form redox system on the surface of the photocatalyst [3]. In fact, this topic has been overdressed in the literature and ends up with much hope and doubt regarding its large scale application. Photocatalysis in theory, is considered as a green technology which can destroy totally organic pollutants into CO_2 and minerals in water. However, in operation, several technological issues have been raised which limit its application as an alternative approach instead of existing technologies [4]. In terms of photonic proprieties of photocatalytic materials, several approaches can be used to boost the visible light response or decrease the rate of e^-/h^+ charges through doping [5], fabrication of heterojunction systems [6], defect engineering [7], crystal phase engineering [8]. However, by comparing the kinetics of photocatalytic technology with some other advanced oxidation approaches, i.e., Fenton or photo-Fenton, it can be deduced easily that photocatalysis exhibits very slow kinetics due to the limited mass transfer. At early stage, many scientific leaders in photocatalysis suggested the use of photocatalytic materials with lower adsorption ability in order to avoid the screen effect problem, wherein, the pollutant molecules can cover the photocatalytic nanoparticles and limit the penetration of light into the surface of the photocatalyst suppressing or decreasing the generation of redox system on the surface. It was believed that the high adsorption of pollutant could counter against the continuous photooxidation process. In addition, it was reported that the adsorption of smaller quantities of the pollutant is necessary as the photocatalytic oxidation by photogenerated reactive oxygen species and directly via positive holes takes place on the surface on the

* Corresponding author.
E-mail addresses: ridha.djellabi@urv.cat, ridha.djellabi@yahoo.com (R. Djellabi).

https://doi.org/10.1016/j.ultsonch.2023.106550
Received 16 June 2023; Received in revised form 1 August 2023; Accepted 2 August 2023
Available online 6 August 2023

photocatalyst. Even though, this trade-off is obtained, the highest performance that fits the large scale requirement is not reached yet. Many recent reports have been published to discuss and bridge the transfer of photocatalytic technology to real world use. Loeb et al. discussed the photocatalytic technology from different sides and they pointed out that the development of pilot reactors for niche applications is still required, and in addition, they stressed that the improvement of photocatalytic efficiency can further be studied by considering the cost and availability of materials [9]. Recently, Djellabi et al. discussed the technological issues of photocatalysis from the materials point of view, along with SWOT analysis to facilitate its transfer to real application. In terms of materials design, the authors reported that the use of low cost approaches to design large amount of highly photoactive materials is much recommended [10,11]. The combination of adsorptive materials and photoactive nanoparticles is regarded as one of the solutions to boost the mass transfer from one site and to reduce the release of by-products into the solution. This process is so-called Adsorb & Shuttle, wherein the adsorptive area plays the role to accumulate pollutant species on the surface nearby photoactive NPs to be oxidized by photogenerated ROSs. The process also ensures the self-cleaning of the surface, allowing further adsorption of pollutants in a continuous system. Several Adsorb & Shuttle based materials have been reported towards the photocatalytic removal of inorganic and organic pollutants such as TiO_2-montmorillonite [12], CuO-Montmorillonite [13], TiO_2-lignocellulosic biomass [14], $BiPO_4$-smectite [15], Ag_3PO_4-Activated carbon [16] and so on. In such type of materials, a synergistic effect combining the adsorption and photoactivity is usually obtained [17]. In addition, many reports demonstrated the enhancement of visible light responsiveness and charges separation when semiconductor NPs are coated on the surface of adsorptive materials via interface interaction, i.e., formation of Ti-O-C bonds between TiO_2 and biomass [18].

Apart from the photocatalytic materials design, the valorization of biomass waste into valuable materials has become a hot research and industrial trend nowadays as it fits with the circular economy concept [19,20]. In short, circular economy is the closed-loop concept which involves the use of renewable energies and boosts the recycling of wastes as well as limits the usage of natural resources. Biomass wastes are considered as the largest worldwide renewable energy resource with about 1800 billion tonnes produced per year. However, less than 3% out of it is used at large scale. Up to date, the conversion of biomass into valuable products needs further investigation and wider large scale investments for various utilizations. The production of activated carbon from biomass towards environmental remediation has been widely suggested by the scientific community, a pool of studies has been reported discussing the conversion of different biomass waste and the optimization of carbonization factors and approaches as reviewed by many reports [21–23].

The present work aims to prepare activated carbon from biomass and then coating it with g-C_3N_4 to be used for the removal of organic pollutants from water. Since the coating of activated carbon by semiconductor nanoparticles has a direct effect on the performance of the composite, herein, we studied comparatively the ball milling and ultrasonic coating approaches. In-situ formation of g-C_3N_4 on the surface of adsorptive materials is difficult to obtain by direct condensation of urea or melamine, and the presence of interfering materials may affect its condensation process. Therefore, two steps synthesis could be more effective to produce g-C_3N_4 coated activated carbon. Three activated carbon/g-C_3N_4 composites were produced by different techniques, namely physically (AC-CN@Phy), ultrasonic (AC-CN@US) and ball milling (AC-CN@BM). The effect of coating approach on the structure, the morphology, the distribution of g-C_3N_4 on the AC were studied and discussed. The photocatalytic performance of different samples was studied for the removal of ciprofloxacin under solar light. The operating parameters and stability of materials were studied as well.

2. Materials and methods

2.1. Experimental

2.1.1. Synthesis of materials

Activated carbon was prepared by the chemical activation method using phosphoric acid (H_3PO_4, 85%) as an activating agent. A brief description of the preparation and activation procedures is as follows: 10 g of date stone biomass waste was impregnated with phosphoric acid (85%) at room temperature. The system was heated in a microwave until its puissance reached 540 w under N_2 atmosphere. After the activation process, the sample was leached with (2 M) NaOH solution to remove the excess of acid, filtered and repeatedly washed with distilled water until the pH of filtrate reached (6–7). The activated materials were then carbonized at 270 W for 8 min under N_2 atmosphere. g-C_3N_4 was been obtained by the calcination of urea at 500 °C for 2 h. AC/g-C_3N_4 composite was prepared by different methods. (i) A mixture of AC and g-C_3N_4 was ball milled at 500 rpm for four cycles of 15 min, resulting in ultrafine light-Black powder (AC-CN@BM). (ii) A mixture of AC and g-C_3N_4 was stirred in ethanol for 1 h, followed by ultrasonic treatment for 1 h at a frequency of 40 KHz (AC-CN@US). For comparison, a composite sample was prepared by physical stirring in the presence of ethanol and without ultrasonic treatment.

2.1.2. Photocatalytic tests

The photocatalytic experiments were carried out in a suntest CPS + ATLAS reactor, providing an irradiation with wavelengths ranging from 300 to 800 nm. The intensity of light irradiation was selected at 250 W/m^2 during the photocatalytic experiments. 25 mg of the sample is dispersed in 100 mL of 30 mg/L Ciprofloxacin (≥98%) solution. During the degradation, 1.5 mL of suspension was withdrawn at selected time intervals and filtered with a 0.45 μm membrane filter. The concentration of Ciprofloxacin was determined by UV–VIS spectrophotometer at the wavelength of maximum absorbance (278 nm).

3. Results and discussion

3.1. Characterization

XRD spectra of AC, bare g-C_3N_4, AC-CN@Phy, AC-CN@US and AC-CN@BM are shown in Fig. 1. X-ray diffractogram of AC shows two main peaks. The intense peak at 2θ of 20–30° is due to the C (002)

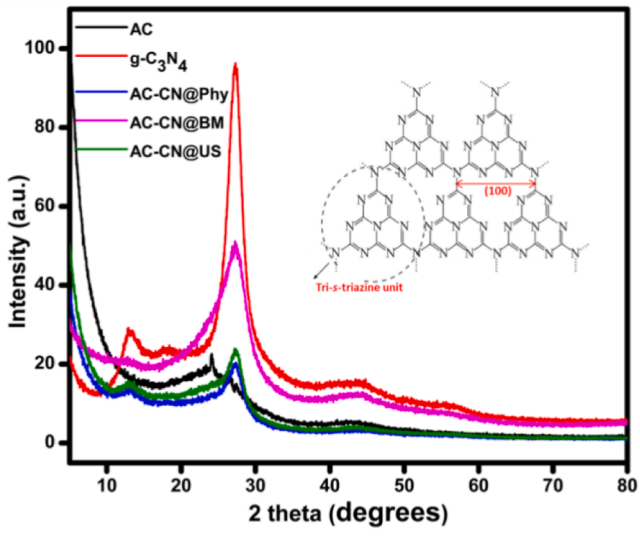

Fig. 1. XRD patterns of bare AC, bare g-C_3N_4, AC-CN@Phy, AC-CN@US and AC-CN@BM.

amorphous carbon structures , while the weaker band at 40–50° represents the C (1 0 1) graphite structure. These two peaks are characteristics of activated carbon [24,25]. Bare g-C_3N_4 X-ray diffractogram shows two distinct diffraction peaks at 27.4° and 13.04° suggesting the successful thermal condensation of urea into hexagonal phase of g-C_3N_4 (JCPDS 87–1526) [26]. g-C_3N_4 is composed of tri-s-triazine building units. The peak at 13.04° (1 0 0) is characteristic for in-plane structural repeating motifs. However, the peak at 27.4° (0 0 2) is due to the interlayer stacking reflections of the aromatic systems [27,28]. Both peaks are significantly intense in bare g-C_3N_4. It can be noticed that the intensities of (0 0 2) and (1 0 0) were reduced in AC-CN@Phy and AC-CN@US. The preparation of these two samples requires the use of ethanol to mix AC with g-C_3N_4. The physically prepared sample is simply dried after the mixing, while AC-CN@US sample is subjected to ultrasonic treatment for 1 h. The decrease in the intensity of peaks as compared to bare g-C_3N_4 or even to the sample prepared via ball milling route is due to solvent exfoliation of g-C_3N_4 which transforms g-C_3N_4 bulk to laminated structure [29,30]. Ethanol has been proved to be excellent solvent for the exfoliation of g-C_3N_4 [31]. In addition, ultrasonic process become common route for the exfoliation of g-C_3N_4 in order to enhance the photoactivity or/and to allow the fixation of other semiconductor nanoparticles on its surface [32–34]. The ultrasonic waves produce heat and pressure which work cooperatively to transform bulk g-C_3N_4 into thinner layers. The combination of solvent and US power would boost the exfoliation of g-C_3N_4 as a result of synergistic effects. The physical effect of cavitation can help the penetration of solvent within the interlayer of g-C_3N_4. And on top of that, the produced heat and microjets can provoke the g-C_3N_4 exfoliation or/and assist the solvent exfoliation. In fact, similar to graphite, g-C_3N_4 is a multilayer based structure. Each layer, as shown in the insert of Fig. 1, is formed via strong covalent bonds between N and C atoms. Whilst, the connection of layers takes place via weak van der Waals force wherein layer to layer distance is about 3.3 nm [35,36]. Therefore, chemical or physical routes could destroy inter-layer based bonds to dissociate g-C_3N_4 bulk. In terms of AC-CN@US sample, another scenario could take place. In fact, the (0 0 2) peak at 27.4° was reduced logically because there is less content of g-C_3N_4 in AC-CN samples as compared pure g-C_3N_4. However, in terms of AC-CN@Phy, it can be noticed that the peak of (2 0 0) crystal planes, is more intense which suggests that g-C_3N_4 is not exfoliated into laminated structure. In addition, the peak of (1 0 0) crystal planes was almost disappeared which probably led to shorter g-C_3N_4 conjugation.

FTIR spectra recorded on bare g-C_3N_4 and AC-g-C_3N_4 composite materials are shown in Fig. 2. Bare g-C_3N_4 spectrum shows the characteristic peaks of standard g-C_3N_4. The series peaks appeared at the range 1240–1461 cm^{-1} are due to the aromatic C—N stretching vibrations and C═N stretching vibrations [37]. The peak at 810 cm^{-1} is attributed to the breathing mode of s-triazine units [38]. Bands at 3074–3321 cm^{-1} are due N—H stretching terminal NH groups [39]. FTIR spectra of AC-CN@Phy and AC-CN@US samples show as well the basic structure of g-C_3N_4 along with lower peak intensity due to the low quantity. However, in the case of AC-CN@BM, it can be seen that the peaks of aromatic C—N/C═N and s-triazine units at the range 1240–1461 cm^{-1} and 810 cm^{-1} were significantly reduced or deformed. It is worthy to mention that ball milling has been used for the exfoliation of bulk g-C_3N_4 for enhanced photoactivity [40–43]. As above-mentioned, van der Waals force based bonds that associate g-C_3N_4 layers can be easily destroyed by several routes. However, ball milling could have negative effect on the structure g-C_3N_4 by destroying bonds that are responsible for long conjugation [40] as confirmed by XRD and FTIR analysis.

The morphology of composites and g-C_3N_4 distribution was analyzed via ESEM-EDX, respectively. The recorded images are shown in Fig. 3. The morphology of bare activated carbon is shown in Fig. 3(a,b). It can be seen than AC exhibits porous structured surface which could be an excellent host of g-C_3N_4 particles. Fig. 3c shows ESEM image of bare g-C_3N_4 which is composed of aggregated irregular folding structured sheets. Fig. 3,d,e,f show ESEM images for AC-CN@BM, AC-CN@Phy and AC-CN@US, while Fig. 3,g,h,i show EDX mapping imaging for AC-CN@BM, AC-CN@Phy and AC-CN@US, respectively. The table in Fig. 3 shows the chemical composition of the analyzed area of each sample. It can be seen from these images that samples prepared by ball milling and ultrasonic routes showed a relatively homogenous distribution of g-C_3N_4 particles on the surface of activated carbon. Ball milling is common approach to create heterogeneous composites because of the strong mechanical and/or produced heat effects that would initiate bonds between solids. In addition, an excellent distribution is usually obtained. Based on the results of XRD analysis, the ball milling process does not transform bulk g-C_3N_4 into thinner layers g-C_3N_4 as compared to physical and ultrasonic routes because of solvent exfoliation of g-C_3N_4. The only advantage of ball milling in this case is the enhanced distribution of g-C_3N_4 on the surface of AC. Physical route showed unwanted aggregation of g-C_3N_4 particles on the surface of AC even though exfoliation of g-C_3N_4 was noticed because of the presence of ethanol as discussed previously. The recorded ESEM-EDX mapping images on the sample obtained via ultrasonic coating route prove excellent distribution of g-C_3N_4 on the surface of AC. As compared with AC-CN@Phy, it is clear that ultrasonic force was behind the distribution of g-C_3N_4 particle on AC surface. Ultrasonic process is used to control the size of particles and uniformity of their distribution on surfaces. Ultrasonic devices with low frequency operation is preferred due to their ability to provide extreme conditions via cavitation and collapsing of produced bubbles which allows intense surface/interface interactions between energy and matter [44–46]. The collapsing of bubbles on the surface of particles produce hot spots with extreme temperature value up to 5000 °C and high pressure up to 1000 bars which results in a violent acceleration of the nanoparticles (jetting phenomena) with extremely high velocity up to 600 km/h [47]. The chemical composition proves further the better distribution of N atom (from g-C_3N_4) on the surface of samples prepared by ball milling and ultrasonic routes, while in the case of physically prepared composite, the amount of N was less. It is important to mention that these analysis are carried out on randomly chosen area of materials, and the amount of N could be higher if the analyzed an area with accumulated g-C_3N_4. Overall, it could be assumed that ethanol-ultrasonic route ensures a simultaneous exfoliation and in situ uniform coating of g-C_3N_4 on the surface of AC without destroying the structure of g-C_3N_4.

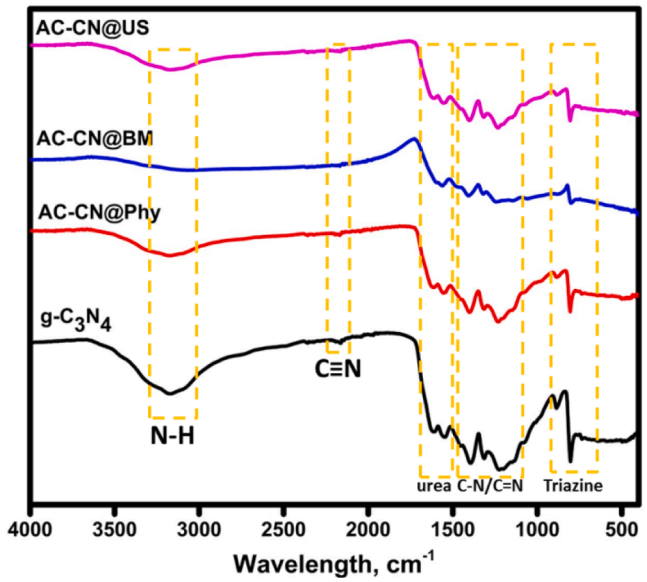

Fig. 2. FTIR spectra of bare AC, bare g-C_3N_4, AC-CN@Phy, AC-CN@US and AC-CN@BM.

TEM images of bare AC, bare g-C_3N_4 and AC-CN@US are shown in Fig. 4. AC exhibits porous structured large particles. Bare g-C_3N_4 is non-

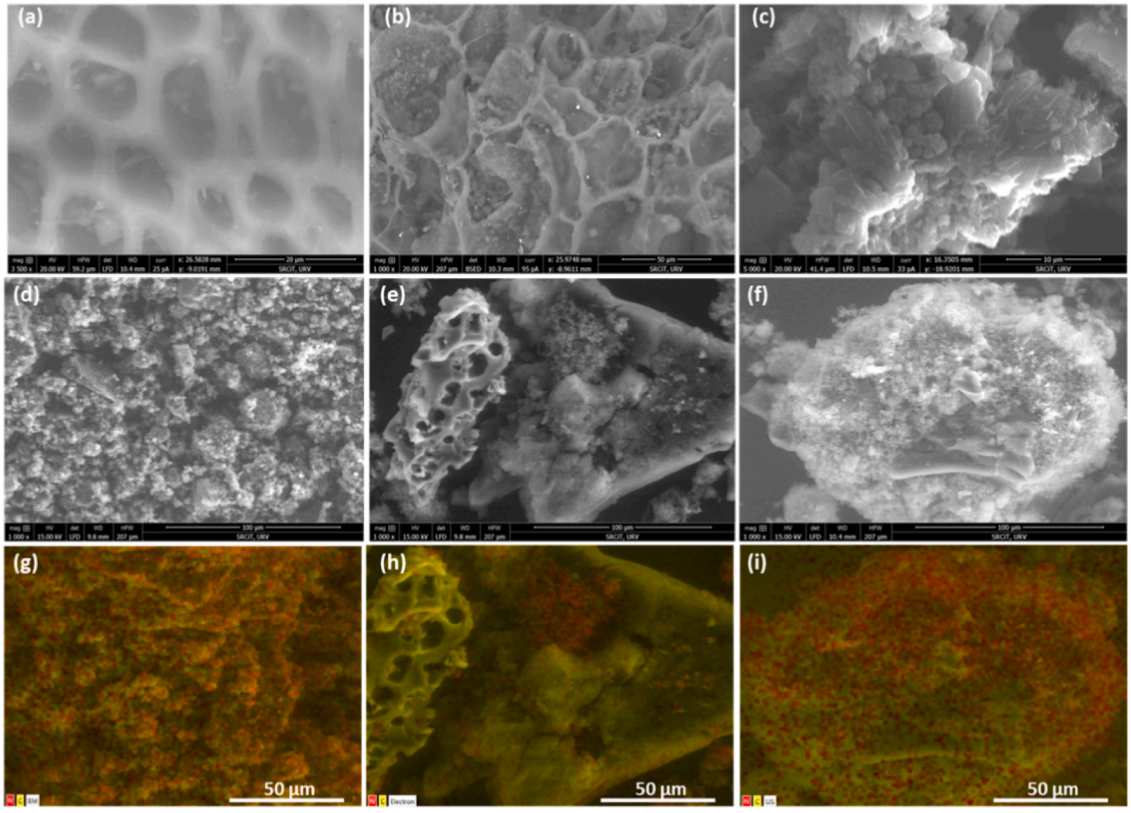

Spectrum Label	AC (Wt%)	CN (Wt%)	AC-CN@US	AC-CN@PHY	AC-CN@BM
C	74.25	35.96	47.75	67.09	50.98
O	19.49	---	13.27	16.24	15.09
N	---	64.04	37.40	11.28	30.68
Na	1.67	---	0.28	1.41	0.61
Si	1.57	---	0.03	---	---
P	2.94	---	1.27	3.98	2.64
Ca	0.08	---	---	---	---
Total	100.00	100.00	100.00	100.00	100.00

Fig. 3. (a) and (b) ESEM images for bare AC, (c) ESEM image for bare g-C_3N_4, (d), (e), (f) ESEM images for AC-CN@BM, AC-CN@Phy and AC-CN@US, respectively. (g), (h), (i) EDX mapping images for AC-CN@BM, AC-CN@Phy and AC-CN@US, respectively. Chemical composition of bare AC, g-C_3N_4 and different composites.

porous laminated two-dimensional sheets. In terms of AC-CN@US, in fact, it is difficult to distinguish AC and g-C_3N_4 in the composite because of the homogenous distribution of g-C_3N_4 on the surface of AC as shown by ESEM images. It can be seen that the activated carbon and g-C_3N_4 are hybridized with each other, suggesting the excellent role of ultrasonic cavitation to link elements and form a homogenous composite at relatively low price. Even though g-C_3N_4 and AC are well connected, the structure of g-C_3N_4 was not affected as confirmed by FTIR and XRD. TEM image at 500 nm shows the small size of g-C_3N_4 sheets which could be due exfoliation by solvent/ultrasound treatment process. The exfoliation can promote the distribution of g-C_3N_4 on the surface of AC.

BET analysis was carried out on bare AC, g-C_3N_4, AC-CN@BM, and AC-CN@US samples and the curves are shown in Fig. 5. Date stone biomass waste was used to prepare bare AC through chemical carbonization using H_3PO_4 as the activating agent. The results show that AC exhibits excellent surface area of 754.75 cm^2/g and pore volume of 0.409 cm^3/g. Bare g-C_3N_4 has a surface area of 56 cm^2/g. The surface areas of AC-CN@BM and AC-CN@US were found to be 114.53 and 328.62 cm^2/g, respectively, suggesting that the ball milling could also destroy the morphology or even push the insertion of g-C_3N_4 particle into block the pores of AC. The pore volumes for AC-CN@BM and AC-CN@US were found 0.037 and 0.174 cm^3/g, respectively. The surface area and pore volume are very crucial in Adsorb & Shuttle based photocatalysts. Therefore, it was concluded that ultrasonic coating of g-C_3N_4 is more advantageous as compared to ball milling route.

PL analysis was carried out on bare g-C_3N_4, AC-CN@BM, AC-CN@Phy and AC-CN@US samples. The curves are shown in Fig. 6. PL analysis can give an idea about the separation of charges. The combination of g-C_3N_4 with carbon materials could reduce the recombination of charges as the AC can play an electron host, resulting in positive holes liberation for the production of ROSs [48]. However, it is important to mention that the separation of charges takes place if there are strong interfacial bonds between the photocatalyst and the supporting adsorbent. The results show that the hybridization of g-C_3N_4 reduces the PL intensity. In fact, the activated carbon is not a photoactive material; therefore, a lower PL intensity is inevitably found when g-C_3N_4 and AC are combined. In terms AC-CN@Phy and AC-CN@US, PL curves seem to have similar manner as compared to bare g-C_3N_4 which further proves

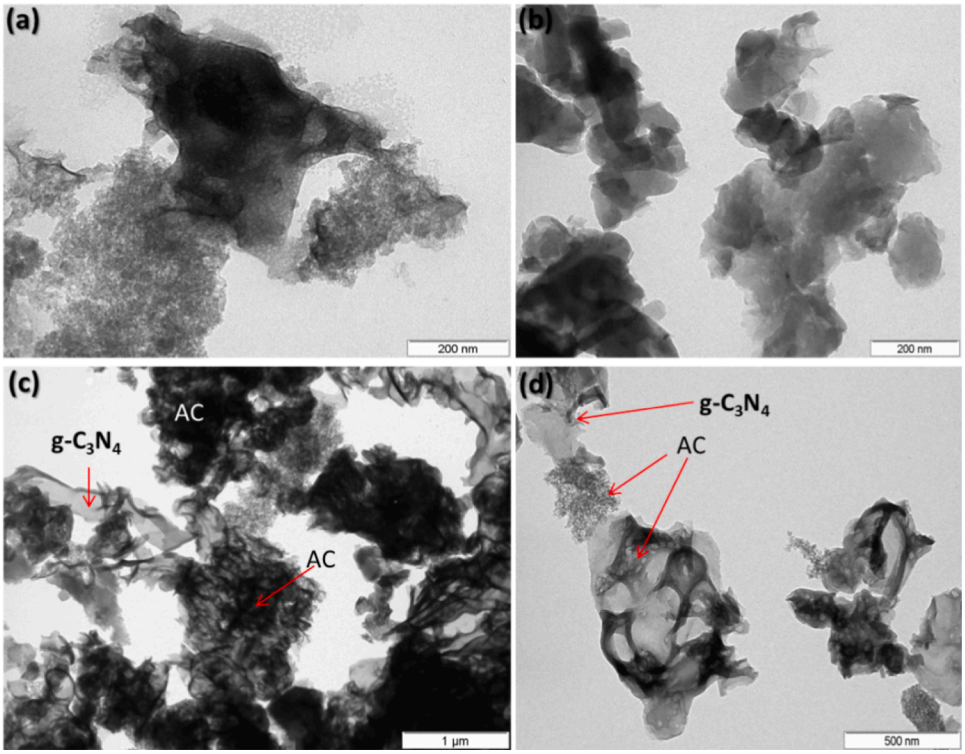

Fig. 4. TEM images of (a) bare AC, (b) bare g-C_3N_4, (c) and (d) AC-CN@US sample at 1 µm and 500 nm, respectively.

that the g-C_3N_4 coated on AC was not damaged. AC-CN@US shows lesser PL intensity compared to AC-CN@Phy, suggesting the good connection between g-C_3N_4 and AC which may help the separation of redox charges. In terms of AC-CN@Phy, the PL intensity is very low. As discussed above, the structure of g-C_3N_4 was destroyed by the effect of BM treatment which leads to limit the photocatalytic activity and charges production.

3.2. Photocatalytic activities

The adsorption and the photocatalytic activities of as prepared materials were studied towards the photocatalytic oxidation of ciprofloxacin under solar irradiation. The results are shown in Fig. 7. As shown in Fig. 7a, bare AC shows an adsorption rate of about 50% within 2 h. Even though the surface area of AC is relatively high, but the functional groups could also play an important role to boost the fixation of ciprofloxacin. It is important to mention that the simple adsorption is not well recommended at large scale as it is a physical transfer of pollutants from liquid phase to solid phase, which then requires the regeneration of the AC to be recycled. Control experiment to check the adsorption of ciprofloxacin on bare g-C_3N_4 was also carried out and a modest adsorption of 20% was found within 2 h. g-C_3N_4 exhibits low surface area, making its photocatalytic performance very slow. Photolysis experiment shows that a decrease in the ciprofloxacin concentration of about 20% under irradiation within 2 h. The photolysis does not lead to mineralize the organic compounds, but mostly it is a partial oxidation or structure modification. In order to enhance the sorption ability, g-C_3N_4 was coated on activated carbon using different approaches. The use of ball milling to coat AC by g-C_3N_4 has led to reduce both the adsorption and photocatalytic ability. As proved by FTIR and XRD analysis, ball milling can destroy the crystal structure of g-C_3N_4 due to the in situ heat produced and physical force. In addition, the surface area of AC-CN@BM was reduced because of several factors such as the degradation of pores of activated carbon as well as their blockage by g-C_3N_4 deposition particles due the intense ball milling effect. Physically prepared sample showed better adsorption and photocatalytic activities than bare g-C_3N_4 and AC-CN@BM sample. In this case, the physically prepared composite could exhibits both adsorption and photocatalytic activities, but in separate manners, wherein there is no synergism between them as the connection between activated carbon and g-C_3N_4 could be weak. In addition, the non-uniformity of g-C_3N_4 on the surface of activated carbon, as shown by SEM-EDX analysis, could limit the synergistic removal of ciprofloxacin. AC-CN@US sample shows the best performance in terms of adsorption and photocatalytic activities. The highest photocatalytic removal was found to be twice higher than bare g-C_3N_4. Indeed, g-C_3N_4 can produce maximum separated charges and also reactive oxygen species on its surface, however, not only ROSs production is important in photocatalytic oxidation process, but also the mass transfer which allows consuming the photoproduced ROSs. From the synthesis point of view, the use of ultrasonic cavitation was found to be perfect approach to design g-C_3N_4 coated activated carbon because of the synergetic cavitation physical, thermal and chemical forces. In short, ultrasound is able to create bubbles in the medium via nucleation of pre-existing dissolved gas bubbles, which their collapsing results in three dominant effects. The ultrasonic waves assist the growth of bubbles consuming all types of gases in water and also the in situ produced water vapor till a critical size to be collapsed in bulk water (known as symmetrical bubble collapse) or on the surface of solid particles (known as asymmetrical bubble collapse) [46]. The collapsing of bubbles in bulk water leads to produce highly physical shock waves, allowing excellent mass transfer which helps the distribution of g-C_3N_4 particles on the surface of activated carbon. The violent collapse of bubbles produces as well high local temperature and pressure up to 5000 K and 1000 atm [19], which might assist to strengthen the fixation of g-C_3N_4 on AC. In addition, bubbles collapse at the interface of solid particles leads to generate a high-speed liquid microjet with velocities up to 100 m/s, in which such energy is concentrated at a particular point of the material. This latter effect might help to improve the porosity, solvent exfoliation of g-C_3N_4, and limits the aggregation of g-C_3N_4. It is important to mention that the applied frequency is a determinant role for governing

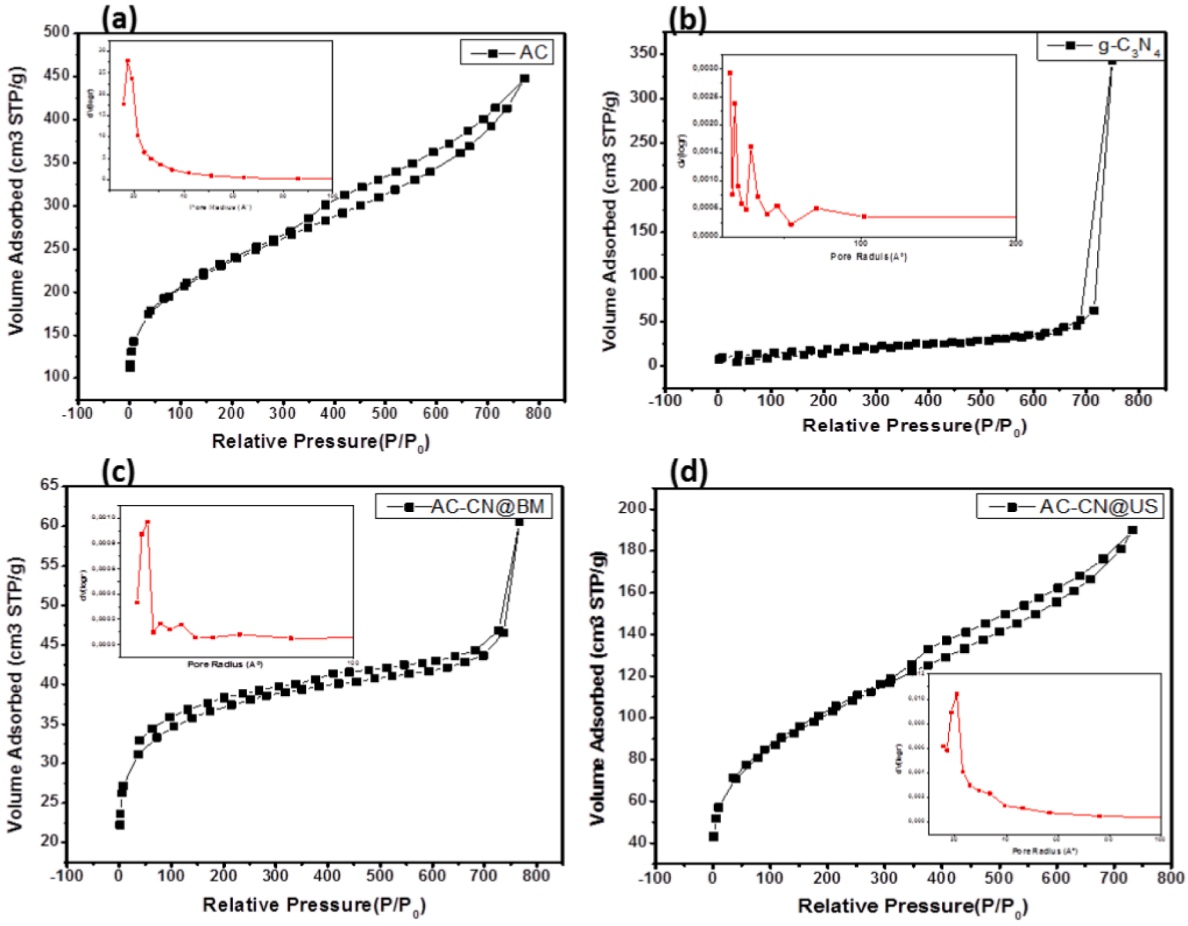

Fig. 5. N_2 adsorption/desorption analysis for (a)AC, (b) g-C_3N_4, (c)AC-CN@BM, and (d)AC-CN@US samples.

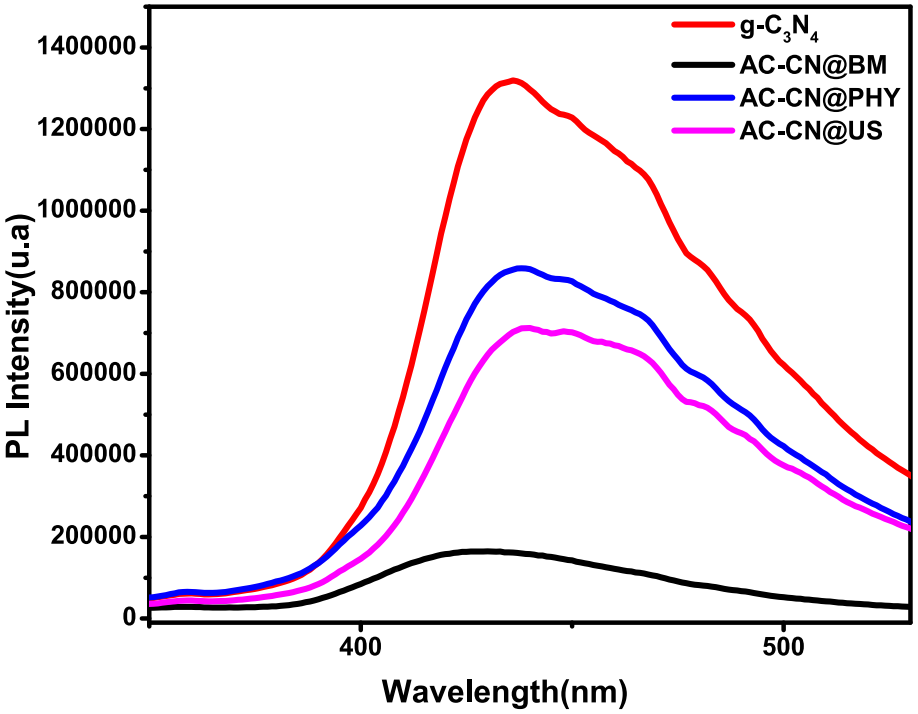

Fig. 6. PL analysis of bare g-C_3N_4, AC-CN@BM, AC-CN@Phy and AC-CN@US samples.

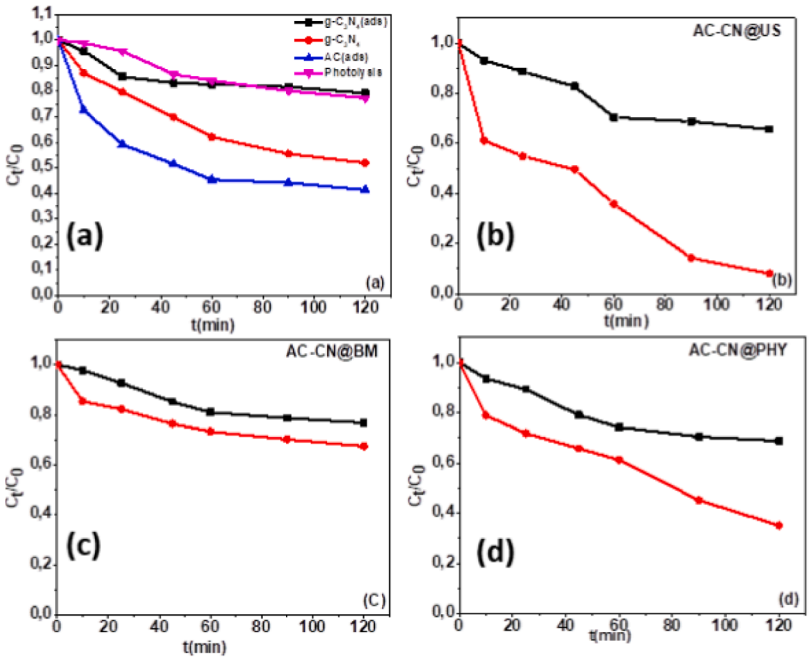

Fig. 7. (a) Photolysis, adsorption on bare AC, adsorption and photocatalytic oxidation of Ciprofloxacin by bare g-C_3N_4. (b), (c) and (d): adsorption (black line) and photocatalytic oxidation (ref line) by different composites, mass of photocatalyst: 0.25 g/L, pH 6.8, [Ciprofloxacin]: 30 ppm.

the cavitation effects. At low frequency, big sized bubbles are produced with lower number, while at higher frequency the reverse is true. Big size bubbles are likely to develop physical effects are dominant include the production of intense shove waves and local heat. The produced heat can split water into reactive oxygen species (ROSs), but their concentration in the medium is less because of the low number of bubbles. The more the frequency, the more the number of bubbles and produced ROSs are, as well as lower physical effect. Herein, a frequency of 40 kHz was used, which provides a dominant physical effect.

Apart from comparing the synthesis routes, the purpose of this material design is the optimization g-C_3N_4 coated activated carbon, keeping excellent g-C_3N_4 distribution and composite porosity as proved by above-discussed characterization analysis. The combination of sorbing domain and photoactive domain was reported by many studies as an excellent approach to obtain highly active materials for pollutants removal, and also boosts the total mineralization [12,49,50]. In small surface area based photocatalysts, the photocatalytic process is very slow because of low mass transfer and the photonic nature of the reaction. In general, the cycle adsorption and radical oxidation needs improvement to make faster and more effective. By assuming that the naked photocatalyst, such as g-C_3N_4, adsorbs high yield of pollutant species, the photocatalytic oxidation process could be inhibited as the particles of photocatalyst are covered with pollutants molecules, limiting the photoexcitation (screen effect) and ROSs generation. In the common scenario, a little quantity of pollutant is adsorbed, followed by radical oxidation, while the release of by-products requires another re-adsorption to reach the final mineralization. The adsorption affinity of different pollutants on the surface of naked also might affect significantly the radical oxidation. Based on the above mentioned discussion, the design of composites, that combine adsorptive and photoactive areas, can synergistically promote the removal of pollutants via the so-called Adsorb and Shuttle process. In this system, the adsorptive area works to concentrate the pollutants species on the surface of composite, nearby the photoactive deposited particles. In this manner, the screen effect is suppressed because the adsorption mostly takes place on the non-photoactive area. From one side, the mass transfer is significantly enhanced to boost the photocatalytic radical oxidation, and from another side, the pollutant species and their by-products can remain longer on the surface of the composite to be further oxidized. The oxidation of pollutant species on the surface of the activated carbon by photoactive g-C_3N_4 allows at the same time the continuous cleaning of the surface, suggesting a cooperative and continuous process. Due the cooperation of photocatalytic and adsorption, Adsorb and Shuttle Process based composites have longer life time and present several pros, on top to the efficiency, such as the low cost, easy separation after the treatment and less generation of by-products. The coating of photocatalytic nanoparticles on photothermal based supports, such as activated carbon, would benefit from the photogenerated local heat which might boost the photocatalytic activity through different ways. Activated carbon is known to be a blackbody solar absorber and photothermal light to heat conversion which can enhance the mass transfer pollutant species and ROSs attack [51,52].

The effect of pH on the adsorption and photocatalytic removal was studied at three pH values, 4, 7 and 10 using AC-CN@US (Fig. 8**a**). At pH 4, it can be seen that the adsorption is quite dominate to remove ciprofloxacin from water, while the contribution of photocatalytic oxidation was about 7%. At acidic pH, the adsorption is high because of the enhanced electrostatic attraction between negatively charged ciprofloxacin species and protonated positive surface of AC-CN@US. Even through, the adsorption was higher, but the photocatalytic activity was low which could be due to the low yield of OH^- which reduces the production of $HO^{\bullet}$ radicals. At pH 7, the photocatalytic activity was the highest and almost three times higher than the adsorption. At this pH range, a tradeoff between the adsorption and photocatalytic oxidation of ciprofloxacin on the surface of AC-CN@US could be obtained, suggesting a fast removal of ciprofloxacin from water. It is important to mention that the adsorption and photocatalytic activity work cooperatively to make the Adsorb and Shuttle process into action. Because the photo-produced ROSs remain mostly on the surface of the photocatalyst, adsorbed pollutant species are subjected to fast oxidation as compared to species at the diffusion layer or in the bulk water. At higher pH, the adsorption was very low which could be due to the electrostatic

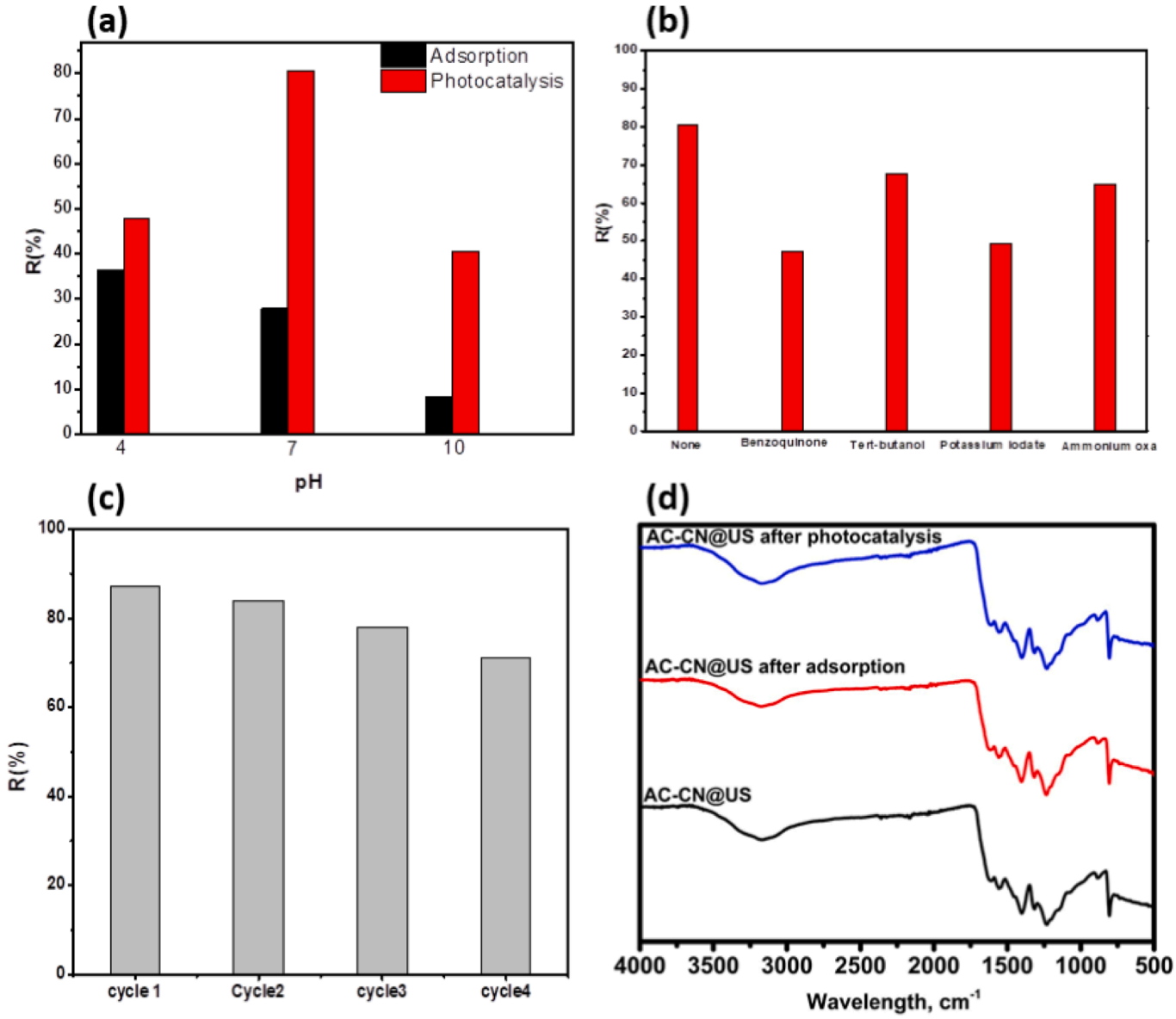

Fig. 8. (a) Effect of pH on the photocatalytic oxidation of ciprofloxacin by AC-CN@US, (b) effect of the addition of scavenging agents. s(c) Recycling tests and (d) FTIR spectra of AC-CN@US before and after adsorption and photocatalytic experiments.

repulsion between ciprofloxacin species and negatively charged AC-CN@US surface. On the contrary, the radical oxidation was quite high as compared to dark adsorption as a result of the fast production of HO˙ radicals from adsorbed HO– species. However, due to the low adsorption, the yield of removal by photocatalytic system is relatively low. Fig. 8**b** shows the effect of scavengers to understand further the mechanistic pathways and the role of different ROSs toward the oxidation of ciprofloxacin. It is important to mention that the scavenging tests are not very convincing to check the activities of different ROSs in photoactive/adsorptive composites since the scavenging molecules could be adsorbed on the surface of AC rather than interact with different ROSs or directly with photogenerated e^-/h^+ charges. The results showed that scavenging of $^{-}\dot{O}_2$ species reduces the oxidation the most, which means that these species participate significantly to oxidize ciprofloxacin molecules. In addition the scavenging of photoproduced electrons via the addition of potassium iodate diminishes as well the oxidation process because the photoproduced electrons are responsible for the generation of $^{-}\dot{O}_2$ species. The quenching of ˙OH using *tert*-butanol as a scavenger led to reduce as well the oxidation of ciprofloxacin, but with lesser rate compared to the case of $^{-}\dot{O}_2$ scavenging. Likewise, the addition of ammonium oxalate, as positive holes scavenger, does not affect significantly the oxidation of ciprofloxacin. Recycling tests were carried out using AC-CN@US, and the results (Fig. 8c) confirm the good stability if the photocatalyst as it can be recycling for five times without significant decrease in the effectiveness. To check further the stability of AC-CN@US and the possible release of g-C_3N_4 from AC, FTIR analysis was carried out after adsorption and photocatalytic experiments, and the results are shown in Fig. 8d. Clearly, it can be seen that the structure and the characteristic peaks of g-C_3N_4 remain in AC-CN@US after adsorption and photocatalytic experiments, proving the significant fixation of g-C_3N_4 on the surface of AC.

4. Conclusions

The present study reports the comparison of three synthesis routes to coat an as-prepared g-C_3N_4 on activated carbon such as physical, ball

milling and ultrasound. Based on the characterization, it was concluded that the ball milling and ultrasonic could lead to well dispersed g-C_3N_4 particles on activated carbon. However, in the case of physical coating, an intense agglomeration of particles on the surface of activated carbon was found. Even though ball milling coating provides excellent particle distribution, it was found that the structure of g-C_3N_4 particles was partially destroyed along with a significant decrease in the surface area which was probably due to the degradation of macrospores of activated carbon or/and their blockage by g-C_3N_4 particles. In terms of photocatalytic activity, AC-CN@BM showed the lowest activity because the photoactive area was partially degraded and also the porosity and surface area were affected. On top of that, the structure of g-C_3N_4 was damaged under ball milling treatment. AC-CN@Phy was more efficient than AC-CN@BM and bare g-C_3N_4 as a result of good adsorption and also photocatalytic radical oxidation. AC-CN@US showed the highest photocatalytic activity, owing to the excellent g-C_3N_4 dispersion and high surface area. Excellent distribution of photocatalytic particles and high surface are important factors to govern the Adsorb & Shuttle process for enhanced removal of organic pollutants. In addition, the cost of starting materials, including biomass waste to prepare activated carbon and urea to prepare g-C_3N_4, as well as an easy and effective ultrasonic route to build the composite might fit with the industrial requirements and sustainable development.

CRediT authorship contribution statement

Meriem Mergbi: Investigation, Conceptualization, Data collection, Methodology. **Dominic Aboagye:** Formal analysis, Investigation, Revision. **Sandra Contreras:** Revision, Funding acquisition, Supervision. **Hedi Ben Amor:** Revision, Conceptualization. **Francisco Medina:** Revision, Funding acquisition, Supervision. **Ridha Djellabi:** Writing, Visualization, Validation, Revision, Supervision.

Declaration of Competing Interest

The authors declare that they have no known competing financial interests or personal relationships that could have appeared to influence the work reported in this paper.

Data availability

No data was used for the research described in the article.

Acknowledgments

Authors are thankful for the support from Grant PID2021-123665OB-I00 and TED2021-129343B-I00 funded by MCIN/AEI/10.13039/501100011033 and, as appropriate, by “ERDF A way of making Europe”, by the “European Union” or by the “European Union NextGenerationEU/PRTR”. Dr. Ridha Djellabi acknowledges Maria Zambrano Grants-2021URV-MZ-15.

References

[1] M. Liras, M. Barawi, Hybrid materials based on conjugated polymers and inorganic semiconductors as photocatalysts: from environmental to energy applications, Chem. Soc. Rev. 48 (2019) 5454–5487.
[2] K. Wenderich, G. Mul, Methods, mechanism, and applications of photodeposition in photocatalysis: a review, Chem. Rev. 116 (23) (2016) 14587–14619.
[3] Y. Nosaka, A.Y. Nosaka, Generation and detection of reactive oxygen species in photocatalysis, Chem. Rev. 117 (2017) 11302–11336.
[4] M.G. Alalm, R. Djellabi, D. Meroni, C. Pirola, C.L. Bianchi, D.C. Boffito, Toward scaling-up photocatalytic process for multiphase environmental applications, Catalysts 11 (2021) 562.
[5] M.R.D. Khaki, M.S. Shafeeyan, A.A.A. Raman, W.M.A.W. Daud, Application of doped photocatalysts for organic pollutant degradation-A review, J. Environ. Manage. 198 (2017) 78–94.
[6] C. Yu, W. Zhou, C.Y. Jimmy, H. Liu, L. Wei, Design and fabrication of heterojunction photocatalysts for energy conversion and pollutant degradation, Chin. J. Catal. 35 (2014) 1609–1618.
[7] S. Bai, N. Zhang, C. Gao, Y. Xiong, Defect engineering in photocatalytic materials, Nano Energy 53 (2018) 296–336.
[8] S. Bai, C. Gao, J. Low, Y. Xiong, Crystal phase engineering on photocatalytic materials for energy and environmental applications, Nano Res. 12 (2019) 2031–2054.
[9] S.K. Loeb, P.J.J. Alvarez, J.A. Brame, E.L. Cates, W. Choi, J. Crittenden, D. D. Dionysiou, Q. Li, G. Li-Puma, X. Quan, D.L. Sedlak, T. David Waite, P. Westerhoff, J.-H. Kim, The technology horizon for photocatalytic water treatment: sunrise or sunset? ACS Publ. 53 (6) (2019) 2937–2947.
[10] R. Djellabi, R. Giannantonio, E. Falletta, C.L. Bianchi, SWOT analysis of photocatalytic materials towards large scale environmental remediation, Curr. Opin. Chem. Eng. 33 (2021), 100696.
[11] R. Djellabi, P. Su, E.A. Elimian, V. Poliukhova, S. Nouacer, I.A. Abdelhafeez, N. Abderrahim, D. Aboagye, V.V. Andhalkar, W. Nabgan, Advances in photocatalytic reduction of hexavalent chromium: From fundamental concepts to materials design and technology challenges, J. Water Process Eng. 50 (2022), 103301.
[12] R. Djellabi, M. Fouzi Ghorab, A. Smara, C.L. Bianchi, G. Cerrato, X. Zhao, B. Yang, Titania–montmorillonite for the photocatalytic removal of contaminants from water: adsorb & shuttle process, Green Mater. Wastewater Treat. (2020) 291–319.
[13] A.N. Saber, R. Djellabi, I. Fellah, N. Abderrahim, C.L. Bianchi, Synergistic sorption/photo-Fenton removal of typical substituted and parent polycyclic aromatic hydrocarbons from coking wastewater over CuO-Montmorillonite, J. Water Process Eng. 44 (2021), 102377.
[14] R. Djellabi, B. Yang, K. Xiao, Y. Gong, D. Cao, H.M.A. Sharif, X. Zhao, C. Zhu, J. Zhang, Unravelling the mechanistic role of TiOC bonding bridge at titania/lignocellulosic biomass interface for Cr (VI) photoreduction under visible light, J. Colloid Interface Sci. 553 (2019) 409–417.
[15] I. Fellah, R. Djellabi, H.B. Amor, N. Abderrahim, C.L. Bianchi, A. Giordana, G. Cerrato, A. Di Michele, N. Hamdi, Visible light responsive heterostructure HTDMA-BiPO4 modified clays for effective diclofenac sodium oxidation: Role of interface interactions and basal spacing, J. Water Process Eng. 48 (2022), 102788.
[16] N. Abderrahim, R. Djellabi, H.B. Amor, I. Fellah, A. Giordana, G. Cerrato, A. Di Michele, C.L. Bianchi, Sustainable purification of phosphoric acid contaminated with Cr (VI) by Ag/Ag3PO4 coated activated carbon/montmorillonite under UV and solar light: Materials design and photocatalytic mechanism, J. Environ. Chem. Eng. 10 (2022), 107870.
[17] M. Mergbi, M.G. Galloni, D. Aboagye, E. Elimian, P. Su, B.M. Ikram, W. Nabgan, J. Bedia, H.B. Amor, S. Contreras, Valorization of lignocellulosic biomass into sustainable materials for adsorption and photocatalytic applications in water and air remediation, Environ. Sci. Pollut. Res. (2023) 1–31.
[18] R. Djellabi, B. Yang, Y. Wang, X. Cui, X. Zhao, Carbonaceous biomass-titania composites with TiOC bonding bridge for efficient photocatalytic reduction of Cr (VI) under narrow visible light, Chem. Eng. J. 366 (2019) 172–180.
[19] R. Djellabi, D. Aboagye, M.G. Galloni, V. Vilas Andhalkar, S. Nouacer, W. Nabgan, S. Rtimi, M. Constantí, F. Medina Cabello, S. Contreras, Combined conversion of lignocellulosic biomass into high-value products with ultrasonic cavitation and photocatalytic produced reactive oxygen species-A review, Bioresour. Technol. 368 (2023) 128333.
[20] N. Abderrahim, M. Mergbi, H.B. Amor, R. Djellabi, Optimization of microwave assisted synthesis of activated carbon from biomass waste for sustainable industrial crude wet-phosphoric acid purification, J. Clean. Prod. 394 (2023), 136326.
[21] A. Funke, F. Ziegler, Hydrothermal carbonization of biomass: a summary and discussion of chemical mechanisms for process engineering, Biofuels Bioprod. Biorefin. 4 (2) (2010) 160–177.
[22] M. Danish, T. Ahmad, A review on utilization of wood biomass as a sustainable precursor for activated carbon production and application, Renew. Sustain. Energy Rev. 87 (2018) 1–21.
[23] W. Ao, J. Fu, X. Mao, Q. Kang, C. Ran, Y. Liu, H. Zhang, Z. Gao, J. Li, G. Liu, J. Dai, Microwave assisted preparation of activated carbon from biomass: A review, Renew. Sustain. Energy Rev. 92 (2018) 958–979.
[24] Z. Xu, T. Zhang, Z. Yuan, D. Zhang, Z. Sun, Y. Huang, W. Chen, D. Tian, H. Deng, Y. Zhou, Fabrication of cotton textile waste-based magnetic activated carbon using FeCl 3 activation by the Box-Behnken design: Optimization and characteristics, RSC Adv. 8 (66) (2018) 38081–38090.
[25] N. Abderrahim, I. Boumnijel, H.B. Amor, R. Djellabi, Heat and ZnCl2 chemical carbonization of date stone as an adsorbent: optimization of material fabrication parameters and adsorption studies, Environ. Sci. Pollut. Res. 29 (2022) 46038–46048.
[26] X.u. Huai, Z. Hang, Z. Wang, D. Liu, Q. Li, Z. He, Y. Chen, X. Han, Efficiently enhancing the photocatalytic activity of g-C3N4 by a simple advanced successive activation method, Micro Nano Lett. 13 (3) (2018) 403–406.
[27] H.-J. Li, B.-W. Sun, L.i. Sui, D.-J. Qian, M. Chen, Preparation of water-dispersible porous gC 3 N 4 with improved photocatalytic activity by chemical oxidation, PCCP 17 (5) (2015) 3309–3315.
[28] P. Su, J. Zhang, K.e. Xiao, S. Zhao, R. Djellabi, X. Li, B.o. Yang, X.u. Zhao, C3N4 modified with single layer ZIF67 nanoparticles for efficient photocatalytic degradation of organic pollutants under visible light, Chin. J. Catal. 41 (12) (2020) 1894–1905.
[29] L.-R. Zou, G.-F. Huang, D.-F. Li, J.-H. Liu, A.-L. Pan, W.-Q. Huang, A facile and rapid route for synthesis of gC 3 N 4 nanosheets with high adsorption capacity and photocatalytic activity, RSC Adv. 6 (89) (2016) 86688–86694.

[30] P. Qiu, H. Chen, C. Xu, N. Zhou, F. Jiang, X. Wang, Y. Fu, Fabrication of an exfoliated graphitic carbon nitride as a highly active visible light photocatalyst, J. Mater. Chem. A 3 (48) (2015) 24237–24244.
[31] Z.G. Liu, J.Y. Wan, Z. Yang, S.Q. Wang, H.X. Wang, Copper phthalocyanine-functionalized graphitic carbon nitride: A hybrid heterostructure toward photoelectrochemical and photocatalytic degradation applications, Chem.–Asian J. 11 (2016) 1887–1891.
[32] W.-J. Long, P. Xu, Y. Yu, F. Xing, C. He, Scalable preparation of high-dispersion g-C3N4 via GQDs-assisted ultrasonic exfoliation for accelerating cement hydration, Cem. Concr. Compos. 134 (2022), 104782.
[33] L. Zhang, F. Huang, C. Liang, L. Zhou, X. Zhang, Q. Pang, Ultrasound exfoliation of g-C3N4 with assistance of cadmium ions and synthesis of CdS/g-C3N4 ultrathin nanosheets with efficient photocatalytic activity, J. Taiwan Inst. Chem. Eng. 60 (2016) 643–650.
[34] H.-Y. Chen, L.-W. Ruan, X. Jiang, L.-G. Qiu, Trace detection of nitro aromatic explosives by highly fluorescent gC 3 N 4 nanosheets, Analyst 140 (2015) 637–643.
[35] M. Groenewolt, M. Antonietti, Synthesis of g-C3N4 nanoparticles in mesoporous silica host matrices, Adv. Mater. 17 (2005) 1789–1792.
[36] J. Fu, J. Yu, C. Jiang, B. Cheng, g-C3N4-Based heterostructured photocatalysts, Adv. Energy Mater. 8 (3) (2018) 1701503.
[37] S. Kappadan, S. Thomas, N. Kalarikkal, Enhanced photocatalytic performance of $BaTiO_3$/g-C_3N_4 heterojunction for the degradation of organic pollutants, Chem. Phys. Lett. 771 (2021) 138513.
[38] S. Pareek, M. Sharma, S. Lal, J.K. Quamara, Polymeric graphitic carbon nitride–barium titanate nanocomposites with different content ratios: a comparative investigation on dielectric and optical properties, J. Mater. Sci. Mater. Electron. 29 (15) (2018) 13043–13051.
[39] Y. Guo, F. Kong, C. Wang, S. Chu, J. Yang, Y. Wang, Z. Zou, Molecule-induced gradient electronic potential distribution on a polymeric photocatalyst surface and improved photocatalytic performance, J. Mater. Chem. A 1 (2013) 5142–5147.
[40] Z. Ma, P. Zhou, L. Zhang, Y. Zhong, X. Sui, B. Wang, Y. Ma, X. Feng, H. Xu, Z. Mao, g-C_3N_4 nanosheets exfoliated by green wet ball milling process for photodegradation of organic pollutants, Chem. Phys. Lett. 766 (2021) 138335.
[41] X. Wei, X. Wang, Y. Pu, A. Liu, C. Chen, W. Zou, Y. Zheng, J. Huang, Y. Zhang, Y. Yang, Facile ball-milling synthesis of CeO2/g-C3N4 Z-scheme heterojunction for synergistic adsorption and photodegradation of methylene blue: characteristics, kinetics, models, and mechanisms, Chem. Eng. J. 420 (2021), 127719.
[42] W. Liu, M. Sun, Z. Ding, Q. Zeng, Y. Zheng, W. Sun, X. Meng, Ball milling synthesis of porous g-C3N4 ultrathin nanosheets functionalized with alkynyl groups for strengthened photocatalytic activity, Sep. Purif. Technol. 282 (2022), 120097.
[43] X. Wang, X. Wang, W. Tian, A. Meng, Z. Li, S. Li, L. Wang, G. Li, High-energy ball-milling constructing P-doped g-C3N4/MoP heterojunction with MoN bond bridged interface and Schottky barrier for enhanced photocatalytic H2 evolution, Appl. Catal. B 303 (2022), 120933.
[44] R. Djellabi, X. Zhao, C.L. Bianchi, P. Su, J. Ali, B. Yang, Visible light responsive photoactive polymer supported on carbonaceous biomass for photocatalytic water remediation, J. Clean. Prod. 269 (2020), 122286.
[45] P. Mohanty, R. Mahapatra, P. Padhi, C.V. Ramana, D.K. Mishra, Ultrasonic cavitation: An approach to synthesize uniformly dispersed metal matrix nanocomposites—A review, Nano-Struct. Nano-Objects 23 (2020), 100475.
[46] D. Meroni, R. Djellabi, M. Ashokkumar, C.L. Bianchi, D.C. Boffito, Sonoprocessing: from concepts to large-scale reactors, Chem. Rev. 122 (2021) 3219–3258.
[47] D.A. Giannakoudakis, D. Łomot, J.C. Colmenares, When sonochemistry meets heterogeneous photocatalysis: designing a sonophotoreactor towards sustainable selective oxidation, Green Chem. 22 (2020) 4896–4905.
[48] P. Lin, H. Hu, H. Lv, Z. Ding, L. Xu, D. Qian, P. Wang, J. Pan, C. Li, C. Cui, Hybrid reduced graphene oxide/TiO 2/graphitic carbon nitride composites with improved photocatalytic activity for organic pollutant degradation, Appl. Phys. A 124 (2018) 1–11.
[49] R. Djellabi, B. Yang, H.M.A. Sharif, J. Zhang, J. Ali, X. Zhao, Sustainable and easy recoverable magnetic TiO2-Lignocellulosic Biomass@ Fe3O4 for solar photocatalytic water remediation, J. Clean. Prod. 233 (2019) 841–847.
[50] D. Vidyasagar, A. Gupta, A. Balapure, S.G. Ghugal, A.G. Shende, S.S. Umare, 2D/2D Wg-C3N4/g-C3N4 composite as "Adsorb and Shuttle" model photocatalyst for pollution mitigation, J. Photochem. Photobiol. A Chem. 370 (2019) 117–126.
[51] R. Djellabi, L. Noureen, V.-D. Dao, D. Meroni, E. Falletta, D.D. Dionysiou, C. L. Bianchi, Recent advances and challenges of emerging solar-driven steam and the contribution of photocatalytic effect, Chem. Eng. J. 431 (2022) 134024.
[52] Y. Li, Q. Shen, R. Guan, J. Xue, X. Liu, H. Jia, B. Xu, Y. Wu, AC@ TiO 2 yolk–shell heterostructure for synchronous photothermal–photocatalytic degradation of organic pollutants, J. Mater. Chem. C 8 (3) (2020) 1025–1040.